 Human Molecular Genetics, 1999, Vol. 8, No. 8 **1387–1396**

ARTICLE

Functional characterization of the Opitz syndrome gene product (midin): evidence for homodimerization and association with microtubules throughout the cell cycle

Silvia Cainarca[1], Silvia Messali[1], Andrea Ballabio[1,2] and Germana Meroni[1,+]

[1]Telethon Institute of Genetics and Medicine (TIGEM), San Raffaele Biomedical Science Park, Via Olgettina 58 and [2]Università Vita e Salute, 20132 Milan, Italy

Received April 27, 1999; Revised and Accepted June 1, 1999

Opitz syndrome (OS) is a multiple congenital anomaly manifested by abnormal closure of midline structures. The gene responsible for the X-linked form of this disease, *MID1*, encodes a protein (midin) that contains a RING, two B-boxes, a coiled-coil (the so-called tripartite motif) and an RFP-like domain. The tripartite motif is characteristic of a family of proteins, named the B-box family, involved in cell proliferation and development. Since the subcellular compartmentalization and the ability to form multiprotein structures both appear to be crucial for the function of this family of proteins, we have studied these properties on the wild-type and mutated forms of midin. We found that endogenous midin is associated with microtubules throughout the cell cycle, co-localizing with cytoplasmic fibres in interphase and with the mitotic spindle and midbodies during mitosis and cytokinesis. Immunoprecipitation experiments demonstrated the ability of the tripartite motif to mediate midin homodimerization, consistent with the evidence, obtained by gel filtration analysis, that midin exists in the form of large protein complexes. Functional characterization of altered forms of midin, resulting from mutations found in OS patients, revealed that association with microtubules is compromised, while the ability to homodimerize and form multiprotein complexes is retained. We suggest that midin is involved in the formation of multiprotein structures acting as anchor points to microtubules and that impaired association with these cytoskeletal structures causes OS developmental defects.

INTRODUCTION

Opitz G/BBB syndrome (OS; MIM 145410 and 300000) is a multiple congenital anomaly primarily affecting midline structures (1–3). OS is characterized by several clinical features, including hypertelorism, clefts of lip and palate, laryngotracheo-oesophageal abnormalities, hypospadias, imperforate anus and developmental delay. The phenotype is more complex and more severe in males than in females. OS is a heterogeneous disease with both an X-linked (Xp22.3) and an autosomal locus (22q11.2) (4). The two forms of the disease cannot be differentiated on the basis of the clinical phenotype (5).

Recently, we cloned *MID1*, the gene responsible for the X-linked form of OS (6). *MID1* maps to the OS critical region in Xp22.3 and is altered in several OS pedigrees as well as in sporadic cases (6,7). The cloning of the *MID1* murine homologue allowed us to study its expression during development (8–10). Although *Mid1* appears to be transcribed in most tissues during early development, high levels of expression were found at later stages in the central nervous system, in the mucosa of the oropharynx, oesophagus, trachea and larynx, in the stomach, in the gut and in the urogenital system (8). Patterning of these tissues is abnormal in OS patients. In fact, abnormal closure of the facial and pharyngeal processes underlies the labiopalatoschisis and the abnormalities of the trachea/oesophagus, while defective fusion of urethral folds results in hypospadia. The phenomena of apoptosis, cell migration and epithelial–mesenchymal transformation have been reported to be important in the process of oral cavity and foregut development and particularly during palatal fusion (11–13). However, little is known about the molecular mechanisms which govern these processes during normal development and about the stage(s) when the presence of *MID1* is required.

MID1 encodes a putative 667 amino acid protein, midin, containing a RING finger motif, followed by two B-boxes, a coiled-coil and a C-terminal RFP-like domain (6). The tripartite motif (RING, B-boxes and coiled-coil domains) characterizes a subfamily of zinc finger proteins, called the B-box family (14,15). The C-terminal RFP-like domain is found in a subset of these proteins and is also present in proteins lacking the tripartite motif (16,17). These domains are found in different combinations; however, their order from the N- to the C-terminus is conserved in all cases, suggesting an integrated

[+]To whom correspondence should be addressed. Tel: +39 02 215601; Fax: +39 02 21560220; Email: meroni@tigem.it

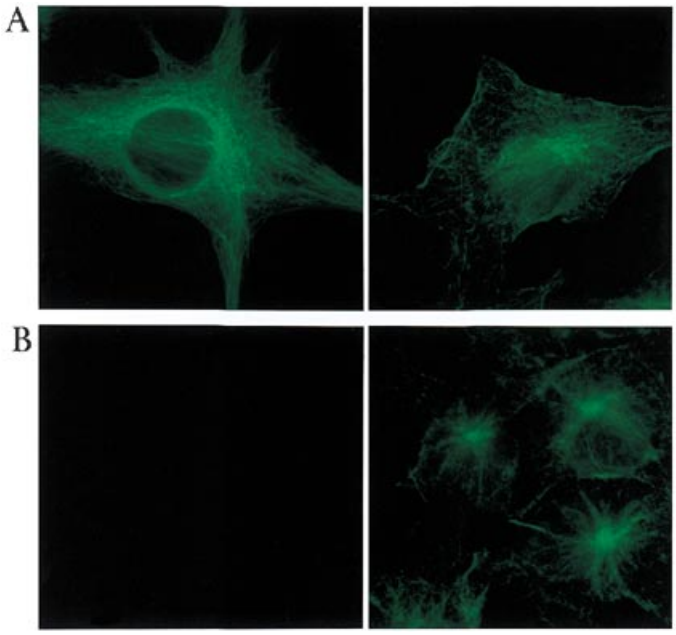

Figure 1. Subcellular localization of endogenous midin. Immunofluorescence was performed using the affinity purified anti-midin antibody followed by FITC-conjugated anti-rabbit antibody. (**A**) A primary fibroblast cell (left panel) and a Cos7 cell (right panel) showing a filamentous signal. (**B**) Cos7 cells treated as above after pre-incubation of the specific antibody with a GST–midin fusion (left panel) and GST (right panel), confirming the specificity of the signal.

rather than a modular function. These genes have been implicated in a variety of processes, such as regulation of development and oncogenesis. Among them, *PML*, *RFP* and *Tif1* acquire oncogenic activity when fused to retinoic acid receptor-α, *RET* and the B-*raf* proto-oncogenes, respectively (18–20). Recently, an additional B-box gene involved in human disease was identified, the *MARENOSTRIN/PYRIN* gene, which is mutated in familial Mediterranean fever (21,22). Although several members of the B-box family have been identified, very little is known about the molecular mechanisms mediating their function, limiting inference about midin's role.

None of the mutations found in the *MID1* gene of OS patients alters the structure of either the RING or B-box domains. All the mutations found to date affect the C-terminal part of the protein including the RFP-like domain. Both missense and insertion/deletion mutations have been found, some of them leading to premature truncation of the protein within the C-terminal portion (6,7).

Here, we report that endogenous midin co-localizes with microtubules. This is in agreement with a recent report describing that overexpressed *MID1* gene product is associated with microtubules, possibly protecting them from disassembling (23). We demonstrated that this association persists throughout the entire cell cycle. Furthermore, we report that midin is able to homo-interact through its tripartite motif and to form large protein complexes within the cell. Finally, we demonstrate that forms of midin reproducing OS mutations are impaired in microtubule binding but retain the ability to homodimerize.

RESULTS

Endogenous midin is associated to microtubules throughout the cell cycle

To investigate the biochemical and cellular properties of midin, we raised rabbit polyclonal antibodies against the N-terminal part of the protein (including the RING and a portion of the B-box1 domain; see Materials and Methods). The antibodies were able to recognize exogenous tagged and non-tagged midin, after transient transfection in Cos7 cells. Indirect immunofluorescence experiments allowed the detection of overexpressed midin in association with cytoskeletal structures (data not shown). Since midin shares a high degree of homology with Mid2 (24), we tested whether the anti-midin antiserum could recognize transiently transfected Mid2 protein, thus impairing endogenous midin analysis. Our antibody was not able to detect Mid2, even when we achieved efficient Mid2 expression, as revealed by the anti-tag antibody (data not shown).

The anti-midin antibody was affinity purified in order to detect the endogenous protein. A cytoskeleton-associated signal was detected in human fibroblasts and in Cos7 cells (Fig. 1A). This signal corresponds to the endogenous midin protein as demonstrated by competition with the GST-fused antigen used to immunize rabbits, and with GST alone as a control (Fig. 1B). We were also able to detect endogenous midin in both rat and murine fibroblasts (data not shown). Mouse midin is, in fact, 97% identical to its human counterpart (8). Previous reports indicated that another member of the tripartite family of proteins, ATDC, was localized to cytoplasmic filamentous structures (25). In particular, ATDC co-localizes with vimentin intermediate filaments. In order to assess with which filaments midin is associated, we used monoclonal antibodies against β-tubulin and vimentin to perform co-localization experiments. We found that midin co-localizes with microtubules, consistent with what was reported recently (23), and only partially overlaps with intermediate filaments, which in Cos7 cells are composed of vimentin (Fig. 2A and B). This partially overlapping distribution is explained by the fact that microtubules and intermediate filaments are often interconnected within cells. The midin signal, as expected, is not coincident with that shown by the actin filaments (data not shown). To confirm the association of midin with microtubules, we treated Cos7 cells with drugs known to disrupt their regular architecture. After treatment with vinblastine, a drug that induces the formation of paracrystalline aggregates of tubulin leading to microtubule depolymerization, midin failed to show its filamentous aspect and the signal was found both dispersed in the cytoplasm and associated with the tubulin paracrystals. A superimposable signal is observed with the anti-β-tubulin antibody (Fig. 2C). The second drug we used, nocodazole, inhibits the addition of tubulin molecules to microtubules with the net effect of microtubule depolymerization. The dispersion of midin, as well as that of the tubulin monomers, is observed within the cytoplasm (Fig. 2D).

Midin is present in association with microtubular structures during all cell-cycle phases. This was demonstrated by immunofluorescence analysis on subconfluent, actively dividing Cos7 cells, where midin is associated with the mitotic spindle during mitosis (Fig. 2E, upper and lower left panels). The midin signal during cytokinesis is observed in the midbodies, presumably in

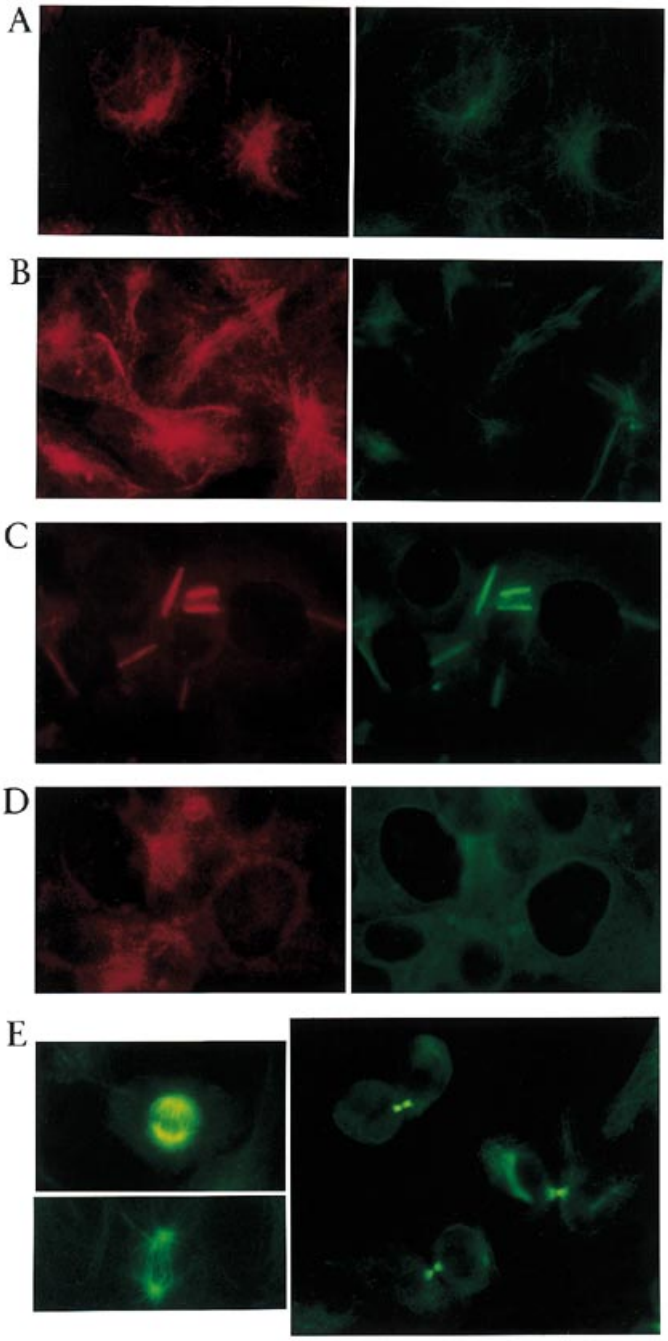

Figure 2. Co-localization of endogenous midin with microtubules in Cos7 cells. (A–D) The left panels show the endogenous midin signal after immunofluorescence with the affinity-purified anti-midin antibody followed by TRITC-conjugated anti-rabbit antibody (red signal). In (A), (C) and (D), the right panels show the double staining with the anti-β-tubulin antibody followed by FITC-coupled anti-mouse antibody (green signal), whereas in (B) the double staining was performed with the anti-vimentin antibody. (**A**) Double staining with anti-tubulin of untreated cells. (**B**) Double staining with anti-vimentin of untreated cells. (**C**) Double staining with anti-tubulin after vinblastine treatment. (**D**) Double staining with anti-tubulin after nocodazole treatment. (**E**) Actively dividing Cos7 cells decorated with the affinity-purified anti-midin antibody followed by FITC-conjugated anti-rabbit antibody showing staining of the the mitotic spindle (upper and lower left panel) and the midbodies (right panel).

association with the remains of the polar spindle microtubules constricted by the contractile ring in the cleavage furrow (Fig. 2E, right panel). Double staining with phalloidin showed that midin is excluded from the region where actin and myosin, which form the contractile ring, are present (data not shown).

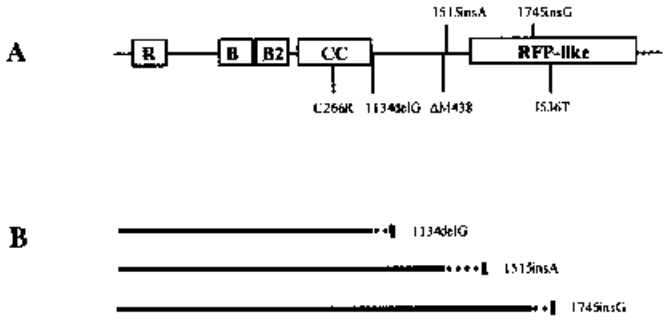

Figure 3. OS mutations reproduced in expression vectors. (**A**) Schematic representation of midin protein structure. The grey squares represent the RING finger domain (R), the two B-box motifs (B1 and B2), the coiled-coil (CC) and the RFP-like domains (RFP-like), respectively. The positions of the OS mutations we recreated *in vitro* are indicated. (**B**) Effects of the point deletion (1135delG) and insertions (1515insA and 1745insG) on the protein structure. The thick lines indicate the length of the putative truncated protein with respect to the above midin structure. The dashed lines correspond to the unrelated amino acid stretch resulting from the out-of-frame mutation event. Five of the mutations were reported elsewhere (6,7); 1515insA is a novel mutation found in OS patients (B. Franco and R. Winter, personal communication).

OS mutants have a decreased affinity for microtubules

By site-directed mutagenesis we have reproduced six of the mutations found in OS patients (6,7; B. Franco and R. Winter, personal communication) (Fig. 3). The cloning of these mutants in appropriate expression vectors allowed us to analyse their distribution within the cells after transient transfection. Although some of the mutants, especially those producing truncated proteins, have a low level of expression, all of them (including missense and truncations) show a cytoplasmic spotted distribution and only partially, and to a variable extent, retain a filamentous distribution. For example, the typical dense pattern of spots obtained with the C266R mutant is shown in Figure 4A. One way to interpret these data is that the mutants diminish their affinity for microtubules. However, the dissociation of the mutant midin molecules from the cytoskeleton has no visible effect on microtubule distribution. In fact, a normal filamentous pattern is observed after double staining with the anti-tubulin antibody (Fig. 4B). When vinblastine was administered to Cos7 cells transiently transfected with the mutant constructs, the specific midin signal was seen to co-localize partially with the tubulin crystal structures, and partially with the spots observed in the untreated cells (Fig. 4C). This behaviour is consistent with the view that the mutants are still able to bind microtubules but presumably with a reduced affinity with respect to the wild-type protein. To exclude the possibility that the filamentous signal we observed was due to the endogenous protein, we used a non-affinity-purified antibody that is not able to detect endogenous midin. Furthermore, the same distribution of the mutants was confirmed using an anti-tag antibody (data not shown).

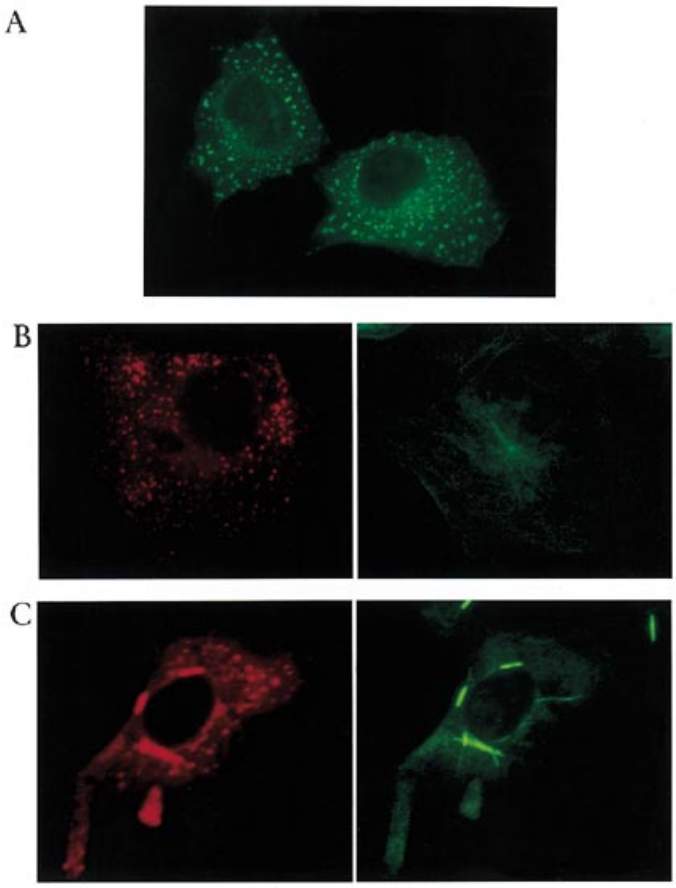

Figure 4. Spotted cytoplasmic signal shown by the C266R OS mutant. (**A**) C266R mutant (Fig. 3) signal after transfection in Cos7 cells and immunostaining with the non-purified anti-midin antiserum followed by FITC-coupled anti-rabbit IgG. (**B**) Double staining with the same antibody as in (A) followed by a TRITC-conjugated anti-rabbit antibody (left panel), and with the anti-tubulin antibody followed by FITC-coupled anti-mouse IgG (right panel). (**C**) The same as in (B) after vinblastine treatment of Cos7 cells.

To identify a putative microtubule-binding domain, we generated tagged expression constructs consisting of several combinations of the midin domains. A schematic representation of these constructs and a summary of the immunofluorescence data are shown in Table 1. The absence of any of the midin domains (RING, B-boxes, coiled-coil and RFP-like) leads to mislocalization of the protein. Nuclear and/or cytoplasmic diffused as well as speckled patterns are observed. Surprisingly, complementary constructs containing non-overlapping portions of midin (i.e. constructs I and M in Table 1) are still able to show a filamentous pattern, although less efficiently than the full-length protein. Taken together, the data on the naturally occurring OS mutants and the artificially mutated constructs do not reveal a specific region responsible for microtubule binding, rather the various domains appear to act together to allow microtubule binding.

Midin homodimerizes

The domains present in midin (RING, B-boxes, coiled-coil and RFP-like) are all thought to be protein–protein interaction interfaces (26–28). For some of the proteins belonging to the tripartite motif family, PML and Xnf7, homo-interaction has been demonstrated (29–31). To test whether midin is able to behave in the same way, two differently tagged *MID1* expression vectors were generated; one bearing a haemagglutinin (HA) tag fused to the N-terminus of midin and the other a Myc tag fused to the C-terminus of the protein (see Materials and Methods). Western blot and immunoprecipitation analyses on transiently transfected Cos7 cell extracts show a band of the expected size (~75 kDa) using the HA-*MID1* and the *MID1*-Myc constructs (lysate lanes of Fig. 5). An additional band of smaller size (marked with an asterisk in Fig. 5) was observed when the *MID1*-Myc construct was used. All these bands were confirmed to correspond to midin by reprobing the same blots with the specific antibody (data not shown). We currently are investigating whether the second band observed with the Myc-tagged construct, proved to be related to midin, is an artefact of transfection or, alternatively, represents a naturally occurring midin modification.

To test for midin–midin interaction, simultaneous transfection of the two tagged constructs in Cos7 cells was performed, followed by immunoprecipitation using either the anti-HA or the anti-Myc antibodies. The HA-midin fusion protein was recovered after immunoprecipitation with the anti-Myc antibody and vice versa (Fig. 5A). Since the HA and Myc tags are not responsible *per se* for the interaction (Fig. 5C), the recovery of the two tagged fusion proteins is due to interaction between two molecules of midin.

We next investigated whether the mutant proteins were able to retain this same property. An analogous scheme was applied, using co-transfection in Cos7 cells of two tagged versions of the mutant proteins. The two missense mutations, C266R and I536T, and two 1 bp insertions leading to premature truncation, 1515insA and 1745insG (Fig. 3), maintained the ability to homo-interact. Figure 5B shows the co-immunoprecipitation of the HA-1745insG and Myc/GFP-1745insG, as an example. It is interesting to note that the 1745insG mutated protein, which retains only one-third of the RFP-like domain, and the 1515insA protein, which completely lacks it, are still able to homodimerize, indicating that this domain is not necessary for midin–midin interaction.

Due to the high homology shared by *MID1* and *MID2* (24), we tested whether or not the two proteins products were also able to interact. HA-*MID2* and *MID1*-Myc constructs have been co-transfected and immunoprecipitations with the anti-HA and the anti-Myc antibodies, respectively, have been performed. Midin is not able to interact with Mid2, as demonstrated in Figure 5C. To exclude that this lack of interaction was due to steric interference caused by the tag system, we verified the results by using Myc/GFP-*MID2* and HA-*MID1* constructs (data not shown). These data confirm that midin homodimerization is not due to mere stickiness of the tripartite motif.

Midin exists in large protein complexes within the cell

In an effort to further evaluate the importance of interactions of midin with itself and possibly with other proteins, we used gel filtration analysis to assess its relative size within the cell. We fractionated a *MID1*-Myc-transfected Cos7 cell S100 supernatant on a Superose 6 column and subsequently performed western blot analysis. As expected, given the ability of midin to interact with itself, we obtained a pattern consistent with elu-

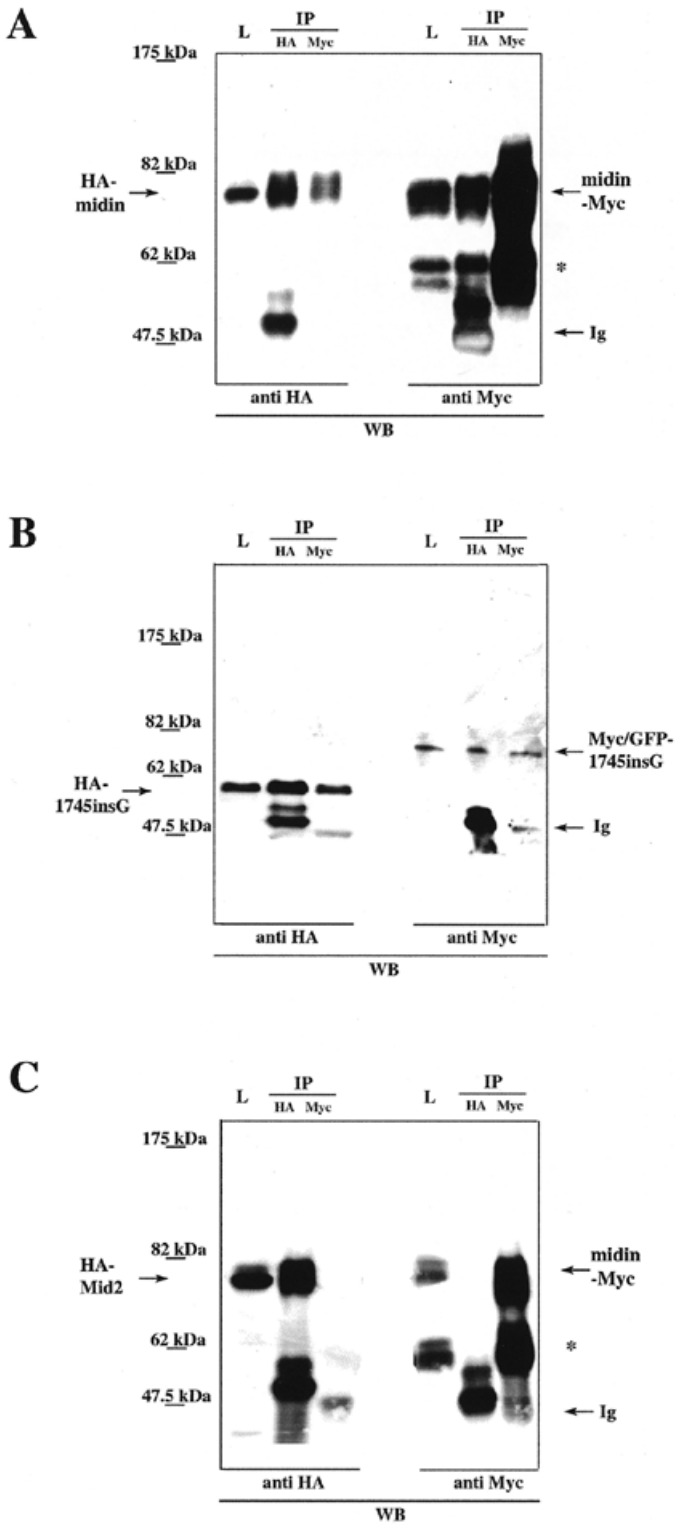

Figure 5. Co-immunoprecipitation experiments showing midin–midin interaction. (**A**) Western blot (WB) analysis using anti-HA and anti-Myc antibodies after immunoprecipitation. The antibodies utilized for the immunoprecipitations are indicated on the top (IP); L, lysate prior to the immunoprecipitation; Ig, immunoglobulins; the asterisk indicates the additional band observed when the *MID1*-Myc construct is transfected; the arrows indicate the bands corresponding to the HA-midin and the midin-Myc proteins. The molecular weights are indicated. (**B**) The same as (A) using the HA-1745insG and Myc/GFP-1745insG mutant fusions instead of the wild-type. (**C**) The same as (A) using the HA-*MID2* and the *MID1*-Myc constructs.

tion of midin at a molecular weight which is higher than that predicted by its deduced amino acid composition. In particular, midin was spread throughout the 232 and 450 kDa range, with the signal also dispersed towards lower molecular weights. It appears that midin may exist as monomers and dimers, but the abundance of midin in the fractions from 27 to 29 indicates a tendency to be contained in larger complexes (Fig. 6, w.t.). When the C266R mutant was analysed using the same method, we observed elution in an overlapping but wider range of fractions with respect to the wild-type. In particular, the immunoreactivity was spread towards the larger sizes (Fig. 6, C266R), and even detected in the exclusion volume corresponding to a molecular size >5000 kDa (data not shown).

Therefore, midin is present in the cell in the form of high molecular weight complexes. At this stage, we cannot rule out the presence of proteins other than midin in these complexes. Moreover, the C266R mutated protein maintained the ability to form complexes, consistent with the fact that it retains homo-interaction properties, and elution even in fractions corresponding to molecular sizes greater than that of the wild-type could reflect an augmented efficacy to interact with itself or with other proteins. It is possible that an increased tendency to form protein aggregates, combined with a diminished association with microtubules, may lead to the formation of the large cytoplasmic structures manifested as spots in immunofluorescence experiments.

DISCUSSION

Based on the expression data and on the anatomical defects present in OS patients, we envisage a possible role for *MID1* in the regulation of cell proliferation, programmed cell death, cell migration or epithelial–mesenchymal transformation. Midin is a member of a family of proteins, the B-box family, sharing the presence of protein–protein interaction domains. Although several proteins belonging to this family are known to be involved in the regulation of cell proliferation and development (19,32–34), very little is known about the cellular and biochemical mechanisms mediating their function. To gain insight into the pathogenetic mechanisms underlying OS, we have undertaken functional studies on the wild-type and mutated forms of midin.

By performing immunofluorescence experiments using affinity-purified antibodies, we were able to detect endogenous midin in several cell lines of human, monkey, rat and mouse origin. In particular, we detected midin in all the human cell types tested, including fibroblasts, kidney epithelial and HeLa cells, consistent with the abundant and widespread distribution of *MID1* mRNA expression observed previously (6,8–10).

The midin signal we observed is compatible with that reported recently (23) on *MID1* transiently transfected cells. Here, we demonstrate that midin shows a cytoplasmic filamentous pattern indistinguishable from that of microtubules. Disruption of the endogenous midin signal using microtubule-depolymerizing agents confirms the association with this cytoskeletal structure. Notably, the physiological expression of midin neither affects microtubule distribution nor protects from drug-induced microtubule depolymerization. Schweiger *et al.* (23) reported that overexpression of midin leads to modification of the microtubule distribution and also protects from colcemid-induced depolymerization. Using a different drug, vinblastine, we found that overex-

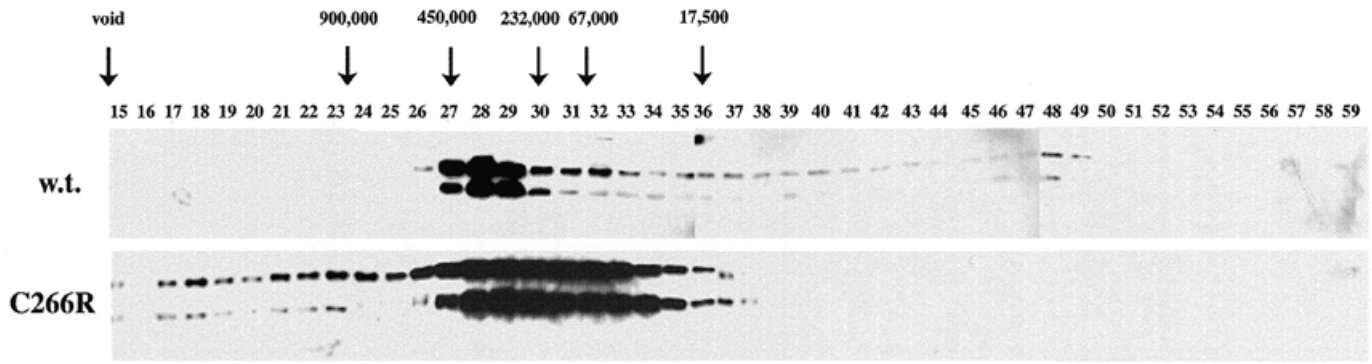

Figure 6. Identification of multiprotein complexes involving the wild-type and C266R *MID1* gene products. Immunoblot analysis, using the anti-c-Myc antibody, of the fractions obtained after gel filtration of *MID1*-Myc-transfected cell lysates. For wild-type midin, immunoreactivity was seen in fractions 26–49 with a peak in fractions 27–29, while for C266R, immunoreactivity was seen in fractions 17–37 with a wider peak in fractions 27–36. The calculated exclusion volume for the columns was at fraction 14. The peaks of elution for various proteins of known molecular weight (Da) are indicated by arrows (900 000 Da corresponds to ferritin dimer; 450 000 Da to ferritin monomer; 232 000 Da to catalase; 67 000 Da to BSA and 17 500 Da to myoglobin).

Table 1. Structure/subcellular localization correlation of various *MID1* constructs

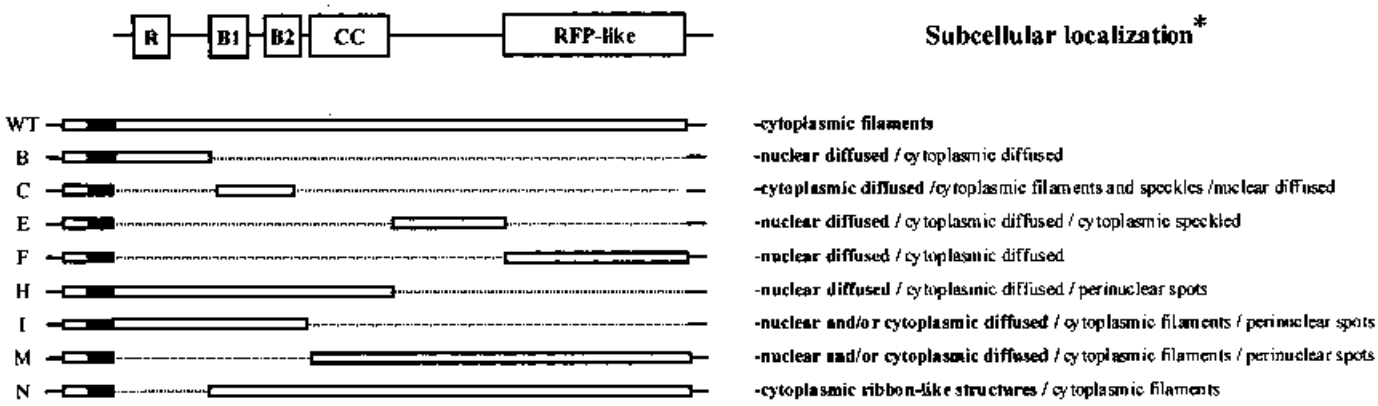

The black bar represents the HA epitope.
*The subcellular localization data have been obtained from immunofluorescence experiments using the anti-HA antibody after transfection of the constructs in Cos7 cells.

pression of Mid1 does not prevent disassembly of microtubules (unpublished data). It is possible that this discrepancy might be due to differences in the mechanisms of action of the distinct depolymerizing drugs (35).

When six of the mutations found in OS patients were analysed, we found a reduced ability to bind microtubules and the tendency to form aggregates. This effect was variable for the different mutations and between individual cells transfected with the same mutated construct. In general, no correlation was evident when missense mutations, rather than truncated proteins, were tested. One of the mutations we analysed (ΔM438) was also reported by Schweiger *et al.* (23). In agreement with that study, we showed that this mutant, as well as the others we tested, forms clumps within the cytoplasm. However, we also observed a residual microtubule distribution associated with both missense and truncation mutations. In fact, none of the Mid1 domains appears to be sufficient and/or necessary to produce a filamentous distribution as revealed by the artificially deleted mutants. This is consistent with the fact that a clear microtubule-binding domain in the correct secondary structure has not been found within the *MID1* sequence. Taken together, these data point towards an indirect mode of binding to microtubules. A possible model for midin association with the microtubular apparatus could involve interaction, through the use of multiple midin domains, with an additional protein (or perhaps more than one) directly bound to the cytoskeleton. Such a model would be consistent with the behaviour of the naturally and artificially occurring mutants, as it does not require the existence of a single domain responsible for microtubule binding.

Preliminary results suggested that the expression of *MID1* is not cell-cycle regulated (unpublished data). Consistently, we have now demonstrated that association of midin with microtubules persists during all cell-cycle phases. In addition to the fil-

amentous interphase pattern of midin distribution, the specific anti-midin antibody decorates spindle fibres during mitosis and also the remains of these fibres forming the midbodies during cytokinesis. It is interesting to note that some of the tripartite motif proteins, such as PML and Tif, displaying a subcellular localization different from that of midin, have been found to be potent growth suppressors (36,37). We do not know yet if midin localization during mitosis has any implications in the regulation of cell proliferation. We found that overexpression of *MID1* is not associated with an inhibition of growth (unpublished data), although we cannot exclude that cells devoid of midin, or containing only a mutated form of midin, might be impaired in their ability to control cell proliferation. Alternatively, the potential ability of midin to control cell growth might be triggered by an as yet unknown stimulus present in midline structures during development. In this respect, a human or a mouse fibroblast cell line harbouring only the mutated gene will be useful to study the effect of the OS mutations on cytoskeleton dynamics and on the control of cell proliferation, without the confounding effect of the endogenous wild-type protein.

There is growing evidence that the RING, B-box and coiled-coil domains are involved in mediating protein–protein interactions which are essential in the formation of multimeric protein complexes (26,27,38). This process appears to be essential for the correct subcellular localization of these proteins (39). Several members of the B-box family, such as Xnf7 and PML, form homodimers and may exist within cells in the form of multiprotein complexes (29–31). Midin appears to behave in a similar way since it is able to interact with itself and is present within cells in the form of large complexes. As these complexes are larger than the predicted size of a midin homodimer, it is possible that they also contain midin multimers and/or heterocomplexes with other as yet unidentified proteins. It is unlikely that Mid2 forms part of the midin-containing complexes as we have demonstrated that the two proteins do not co-immunoprecipitate. Although it is possible that specific modifications are necessary to provoke an interaction between these two closely related proteins, the inability to interact is consistent with the fact that *MID2* has not been found to be mutated in patients with OS (24). It is possible that, considering the high homology and the coincident subcellular localization, Mid2 might act in different tissues or participate in different pathways using the same basic mechanism as midin.

As reported previously for other members of the B-box family, we have found that the tripartite motif is sufficient for midin homo-interaction. Consistently, this property is not affected in the OS mutants that do not involve the RING, B-box and coiled-coil domains. The only possible exception is the C266R mutation that actually falls within the predicted coiled-coil region. A more detailed sequence analysis revealed that the putative coiled-coil sequence is divided into two different regions, the first with a high probability of forming a coiled-coil structure and the second with a considerably lower probability. The amino acid substitution lies exactly between the two regions. It is therefore possible that only the first half of the predicted coiled-coil region adopts a coiled-coil structure, forming the functional tripartite motif together with the RING and the two B-box domains. A similar conclusion was derived for the Rfp protein belonging to this family (P. Freemont, personal communication). If this is indeed the case, the C266R substitution, as with all other mutations identified to date, would fall within the C-terminal functional half of midin.

Midin subcellular localization and mutations are reminiscent of the *GLI3* gene situation. *GLI3* codes for a zinc finger protein that has been found to be involved in three different syndromes, Greig cephalopolysyndactily (40,41), Pallister–Hall (42) and post-axial polydactyly type A (43). There is a perfect correlation between the position of the truncations generated by the frameshift mutations and the syndromes to which they give rise (44). This correlation is also consistent biochemically. In fact, the position of truncation mutations matches perfectly the different subcellular localizations and the different residual transcriptional activities retained by the mutants (45). Notably, the *Drosophila GLI* homologue, *cubitus interruptus* (ci), which is a molecule known to be involved in regulation of development, is also associated with microtubules by indirect anchorage through the costal2 and fused proteins (46,47).

In conclusion, these data support the view that midin is composed of two distinct functional domains, namely the N-terminal half, including the tripartite motif, sufficient to mediate homodimerization, and the C-terminal portion, mainly involved in microtubule association. By forming multiprotein aggregates, midin could create a microtubule-anchored environment to allow the occurrence of protein modifications or to regulate protein shuttling between different cellular compartments. It is possible that mutations in the tripartite motif might either lead to a phenotype different from OS or be lethal. As all mutations found to date in OS patients fall in the C-terminal part of the *MID1* gene, it appears that microtubule association is crucial for midline fusion processes that are compromised in OS.

MATERIALS AND METHODS

Plasmids

MID1 full-length cDNA (6) was cloned into pBS-SK(–) and into several expression vectors. HA-*MID1* was constructed by placing *MID1* cDNA 3' in-frame with the HA epitope into plasmid pCDNA3 (Invitrogen, Leek, The Netherlands); Myc-*MID1* by placing *MID1* cDNA 5' in-frame with the c-Myc epitope into a modified pMT21 vector (48); and c-MYC/GFP-*MID1* by placing *MID1* cDNA 3' in-frame with the c-Myc/GFP tag into plasmid pCDNA3. The artificially deleted *MID1* cDNA constructs presented in Table 1 were created using PCR fragments cloned 3' in-frame with the HA epitope into plasmid pCDNA3. The oligonucleotides used for the PCR assay were: 5'-CAGAATTCATGGAAACACTGGAGTCA (Rf) and 5'-CACTCGAGCTGGAACCTGTCGATGAT (Rr) for construct B; 5'-CAGAATTCCTCAAGCGCAACGTCACC (B1f) and 5'-CACTCGAGGTCATAGCGCTCACTCAA (B2r) for construct C; 5'-CAGAATTCCAGTGCATTGAGCGGTCA (tdnf) and 5'-CACTCGAGAGGCTCACTGCTGCGGCT (tdnr) for construct E; 5'-CAGAATTCATGGTCAAGGCCATCAAC (RFPf) and 5'-CACTCGAGCGGCAGCTGCTCTGTGCA (RFPr) for construct F; the oligonucleotide Rf and the 5'-CACTCGAGGATGAGTGATGCTGACCG (CCr) for construct H; the oligonucleotides Rf and B2r for construct I; 5'-CAGAATTCGATCATCAGGTGGCAGCT (CCf) and the oligonucleotide RFPr for construct M; and the oligonucleotides B1f and RFPr for construct N.

PCR site-directed mutagenesis

Site-directed mutagenesis was performed using the commercially available QuickChange Site-Directed Mutagenesis Kit (Stratagene, La Jolla, CA), in accordance with the manufacturer's instructions. To introduce the C266R, 1134delG, ΔM438, 1745insG, 1516insA and I536T mutations into wild-type *MID1* cDNA, the following oligonucleotides were used: 5'-GAAGATCACGCTCCTCTGTC-3' and 5'-GACAGAGGAGCGTGATCTTC-3' (nucleotides 972–992 of *MID1* cDNA) for the C266R mutation; 5'-GATCATTCTCCTTCAGAGAGTGTTC(–)GCTTGGGAG-3' and 5'-CTCCCAAGCG(–)AACACTCTCGAAGGAGAATGATC-3' (nucleotides 1125–1160 of *MID1* cDNA) for the 1134delG mutation; 5'-GTTGGGTACTAT(–)CCAGCTATCAG-3' and 5'-CTGATAGCTGG(–)ATAGTACCCAAC-3' (nucleotides 1487–1513 of *MID1* cDNA) for the ΔM438 mutation; 5'-GTGAAGCGTTCCAGgTGTGTG-3' and 5'-CACACAcCTGGAACGCTTCAC-3' (nucleotides 1735–1755 of *MID1* cDNA) for the 1745insG mutation; 5'-GTGGTTCTGCTtTGATGTTGGGTAC-3' and 5'-GTACCCAACATCAaAGCAGAACCAC-3' (nucleotides 1504–1528 of *MID1* cDNA) for the 1516insA mutation; and 5'-GCCACTATCAGTAAACACATTTC-3' and 5'-GAAATGTGTTTACTGATAGTGGC-3' (nucleotides 1781–1804 of *MID1* cDNA) for the I536T mutation. In the preceding list, the nucleotide substitutions are underlined, the nucleotide insertions are in lower case and deletions of one or more nucleotides are indicated with the symbol (–). The DNA sequence of each mutant construct was confirmed by sequence analysis. The mutant *MID1* expression vectors were constructed by cloning the mutated *MID1* coding region into plasmids HA-pCDNA3, pMT21 and c-Myc/GFP-pCDNA3, as described above.

Antibodies

The region of amino acids 1–124 of the *MID1* gene product was fused to the GST tag in the bacterial expression vector pGEX2T (Pharmacia Biotech, Uppsala, Sweden) and was produced in *Escherichia coli*, after induction with isopropyl-β-D-thiogalactoside (IPTG). The GST fusion protein was purified on a glutathione–Sepharose 4B column (Pharmacia Biotech) and was used to immunize rabbits. Midin antiserum was first precipitated with ammonium sulfate, then the immunoglobulins were purified on a protein A–Sepharose column (Pharmacia Biotech). Subsequently, the specific anti-midin antibodies were affinity purified using an Aminolink column (Pierce, Rockford, Il) coupled with 10 mg of the GST–midin fusion protein. The following antibodies were also used: anti-β-tubulin monoclonal antibody (clone KMX-1; Boehringer Mannheim, Mannheim, Germany); anti-vimentin (clone V9; Santa Cruz Biotechnology, Santa Cruz, CA); anti-HA monoclonal antibody (clone 12CA5; Boehringer Mannheim); and anti-c-Myc Mab 9E10 antibody (49).

Cell culture and transfection

Cos7 cells and human primary cultured fibroblasts were grown in Dulbecco's modified Eagle's medium supplemented with 10% fetal calf serum, 100 g/ml penicillin and 100 g/ml streptomycin at 37°C in a 5% CO_2 atmosphere.

Transfections were performed by the calcium phosphate method (50). Ten centimeter diameter dishes were transfected with 10 μg cDNA expression vectors for the immunoprecipitation experiments. Chamber slides (8 wells) transfected with 0.5 μg DNA/well were used for the immunofluorescence assays.

Immunofluorescence

Cells were grown on glass coverslips to 50% confluence, incubated with vinblastine (10 mg/ml; Sigma, Munich, Germany) for 2 h, or with nocodazole (10 mM; Sigma) for 1 h or were left untreated. They were rinsed with phosphate-buffered saline (PBS) and fixed with 4% paraformaldehyde for 15 min. The cells were then permeabilized with 0.2% Triton X-100 for 30 min, blocked with porcine serum for 1 h and incubated for 3 h with the antibody. Staining was obtained after incubation for 1 h with fluorescein isothiocyanate (FITC)-conjugated anti-rabbit antibodies alone or with both tetramethylrhodamine isothiocyanate (TRITC)-conjugated anti-rabbit and FITC-conjugated anti-mouse antibodies in the double immunofluorescence experiments. The following antibodies were used: midin antiserum purified on a protein A–Sepharose column (1:500 dilution); affinity-purified anti-midin (1:25 dilution); anti-β-tubulin (0.8 μg/ml final concentration); anti-vimentin (2 μg/ml final concentration); and anti-HA (0.8 μg/ml final concentration). Competition was performed by pre-incubating the primary antibody with 30 μg of either the GST–Mid1 fusion used to generate the antibody, or 30 μg of GST alone as control.

Co-immunoprecipitation

For co-immunoprecipitation experiments, 1×10^7 Cos7 cells transfected either with wild-type or mutant HA-*MID1*, *MID1*-Myc or Myc/GFP-*MID1* constructs were lysed in PBS containing 1% NP-40 and 1× protease inhibitors, sonicated and clarified by centrifugation at 10 000 *g* to remove cell debris. The supernatant was immunoprecipitated with 6 μg anti-HA antibody or 500 μl anti-c-Myc supernatant for 4 h at 4°C and the immunocomplexes collected with protein G–Sepharose beads. The complexes were subjected to 7.5% SDS–PAGE separation and immunoblotting performed as described below.

Immunoblot

Proteins were boiled for 5 min in sample buffer, separated by 7.5% SDS–PAGE and electroblotted on PVDF membranes (Hybond-P; Amersham, Little Chalfont, UK). The membrane was rinsed in methanol and blocked in TTBS, 5% dry milk (TTBS: 20 mM Tris–HCl pH 7, 50 mM NaCl and 0.1% Tween-20). Incubation with the primary antibodies was performed using anti-c-Myc monoclonal antibody supernatant (1:5 diluition) or anti-HA monoclonal antibody (final concentration 0.8 μg/ml) in TTBS, 5% dry milk. Antibody binding was detected with a secondary anti-mouse IgG coupled with horseradish peroxidase, followed by visualization with the Enhanced Chemiluminescence kit (Amersham).

Gel filtration chromatography

After transfection with either wild-type or C266R *MID1*-Myc constructs, confluent Cos7 cells were washed twice in PBS. The cells were then lysed in PBS containing 0.1% NP-40 and 1× protease inhibitors, sonicated and centrifuged at 10 000 *g* at 4°C for 10 min. The supernatant was centrifuged at 100 000 *g*

at 4°C for 30 min. The samples were loaded onto a Superose 6 gel filtration column, on a Pharmacia FPLC system, which was equilibrated with lysis buffer. Column runs were monitored by a UV spectrophotometer at OD_{280} and 0.5 ml fractions were collected. A 15 µl aliquot of each fraction was separated by 7.5% SDS–PAGE and subjected to immunoblot. Four protein standards were used to calibrate the column: ferritin (monomer: 450 kDa; dimer: 900 kDa), catalase (232 kDa), bovine serum albumin (67 kDa) and myoglobin (17.5 kDa).

ACKNOWLEDGEMENTS

We thank Eugenio Monti for helpful technical assistance, Nandita A. Quaderi, Elena I. Rugarli and Alexandre Reymond for critical reading of the manuscript, and Melissa Smith for manuscript preparation. This work was supported by the Italian Telethon Foundation.

REFERENCES

1. Opitz, J.M., Frías, J.L., Guttenberger, J.E. and Pellet, J.R. (1969) The G syndrome of multiple congenital anomalies. *Birth Defects: Original Article Series*, Vol. 5, pp. 95–102.
2. Opitz, J.M., Summitt, R.L. and Smith, D.W. (1969) The BBB syndrome familial telecanthus with associated congenital anomalies. *Birth Defects: Original Article Series*, Vol. 5, pp. 86–94.
3. Cordero, J.F. and Holmes, L.B. (1978) Phenotypic overlap of the BBB and G syndromes. *Am. J. Med. Genet.*, **2**, 145–152.
4. Robin, N.H., Feldman, G.J., Aronson, A.L., Mitchell, H.F., Weksberg, R., Leonard, C.O., Burton, B.K., Josephson, K.D., Laxova, R., Aleck, K.A., Allanson, J.E., Guion-Almeida, M.L., Martin, R.A., Leichtman, L.G., Price, R.A., Opitz, J.M. and Muenke, M. (1995) Opitz syndrome is genetically heterogeneous, with one locus on Xp22, and a second locus on 22q11.2. *Nature Genet.*, **11**, 459–461.
5. Robin, N.H., Opitz, J.M. and Muenke, M. (1996) Opitz G/BBB syndrome: clinical comparisons of families linked to Xp22 and 22q, and a review of the literature. *Am. J. Med. Genet.*, **62**, 305–317.
6. Quaderi, N.A., Schweiger, S., Gaudenz, K., Franco, B., Rugarli, E.I., Berger, W., Feldman, G.J., Volta, M., Andolfi, G., Gilgenkrantz, S., Marion, R.W., Hennekam, R.C.M., Opitz, J.M., Muenke, M., Ropers, H.H. and Ballabio, A. (1997) Opitz G/BBB syndrome, a defect of midline development, is due to mutations in a new RING finger gene on Xp22. *Nature Genet.*, **17**, 285–291.
7. Gaudenz, K., Roessler, E., Quaderi, N., Franco, B., Feldman, G., Gasser, D.L., Wittwer, B., Horst, J., Montini, E., Opitz, J.M., Ballabio, A. and Muenke, M. (1998) Opitz G/BBB syndrome in Xp22: mutations in the *MID1* gene cluster in the carboxy-terminal domain [published erratum appears in *Am. J. Hum. Genet.* (1998) **63**, 1571]. *Am. J. Hum. Genet.*, **63**, 703–710.
8. Dal Zotto, L., Quaderi, N.A., Elliott, R., Lingerfelter, P.A., Carrel, L., Valsecchi, V., Montini, E., Yen, C.-H., Chapman, V., Kalcheva, I., Arrigo, G., Zuffardi, O., Thomas, S., Willard, H., Ballabio, A., Disteche, C.M. and Rugarli, E.I. (1998) The mouse *Mid1* gene: implications for the pathogenesis of Opitz syndrome and the evolution of the mammalian pseudoautosomal region. *Hum. Mol. Genet.*, **7**, 489–499.
9. Palmer, S., Perry, J., Kipling, D. and Ashworth, A. (1997) A gene spans the pseudoautosomal boundary in mice. *Proc. Natl Acad. Sci. USA*, **94**, 12030–12035.
10. Van den Veyver, I.B., Cormier, T.A., Jurecic, V., Baldini, A. and Zoghbi, H.Y. (1998) Characterization and physical mapping in human and mouse of a novel RING finger gene in Xp22. *Genomics*, **51**, 251–261.
11. Pratt, R.M. and Martin, G.R. (1975) Epithelial cell death and cyclic AMP increase during palatal development. *Proc. Natl Acad. Sci. USA*, **72**, 874–877.
12. Fitchett, J.E. and Hay, E.D. (1989) Medial edge epithelium transforms to mesenchyme after embryonic palatal shelves fuse. *Dev. Biol.*, **131**, 455–474.
13. Carette, M.J. and Ferguson, M.W. (1992) The fate of medial edge epithelial cells during palatal fusion *in vitro*: an analysis by DiI labelling and confocal microscopy. *Development*, **114**, 379–388.
14. Borden, K.L.B., Martin, S.R., O'Reilly, N.J., Lally, J.M., Reddy, B.A., Etkin, L.D. and Freemont, P.S. (1993) Characterisation of a novel cysteine/histidine-rich metal binding domain from *Xenopus* nuclear factor XNF7. *FEBS Lett.*, **335**, 255–260.
15. Borden, K.L.B. and Freemont, P.S. (1996) The RING finger domain: a recent example of a sequence–structure family. *Curr. Opin. Struct. Biol.*, **6**, 395–401.
16. Mather, I.H. and Jack, L.J. (1993) A review of the molecular and cellular biology of butyrophilin, the major protein of bovine milk fat globule membrane. *J. Dairy Sci.*, **76**, 3832–3850.
17. Henry, J., Ribouchon, M.T., Offer, C. and Pontarotti, P. (1997) B30.2-like domain proteins: a growing family. *Biochem. Biophys. Res. Commun.*, **235**, 162–165.
18. de The, H., Lavau, C., Marchio, A., Chomienne, C., Degos, L. and Dejean, A. (1991) The PML–RARα fusion mRNA generated by t (15;17) translocation in acute promyelocytic leukemia encodes a functionally altered RAR. *Cell*, **66**, 675–684.
19. Takahashi, M., Inaguma, Y., Hiai, H. and Hirose, F. (1988) Developmentally regulated expression of a human 'finger'-containing gene encoded by the 5' half of the *ret* transforming gene. *Mol. Cell. Biol.*, **8**, 1853–1856.
20. LeDouarin, B., Zechel, C., Garnier, J.M., Lutz, Y., Tora, L., Pierrat, P., Heery, D., Gronemeyer, H., Chambon, P. and Losson, R. (1995) The N-terminal part of TIF1, a putative mediator of the ligand-dependent activation function (AF-2) of nuclear receptors, is fused to B-raf in the oncogenic protein T18. *EMBO J.*, **14**, 2020–2033.
21. The French FMF Consortium (1997) A candidate gene for familial Mediterranean fever. *Nature Genet.*, **17**, 25–31.
22. The International FMF Consortium (1997) Ancient missense mutations in a new member of the *RoRet* gene family are likely to cause familial Mediterranean fever. *Cell*, **90**, 797–807.
23. Schweiger, S., Foerster, J., Lehmann, T., Suckow, V., Muller, Y.A., Walter, G., Davies, T., Porter, H., van Bokhoven, H., Lunt, P.W., Traub, P. and Ropers, H.H. (1999) The Opitz syndrome gene product, MID1, associates with microtubules. *Proc. Natl Acad. Sci. USA*, **96**, 2794–2799.
24. Buchner, G., Monini, E., Andolfi, G., Quaderi, N., Cainarca, S., Messali, S., Bassi, M.T., Ballabio, A., Meroni, G. and Franco, B. (1999) *MID2*, a homologue of the Opitz syndrome gene *MID1*: similarities in subcellular localization and differences in expression during development. *Hum. Mol. Genet.*, **8**, 1397–1407.
25. Brzoska, P.M., Chen, H., Zhu, Y., Levin, N.A., Disatnik, M.H., Mochly-Rosen, D., Murnane, J.P. and Christman, M.F. (1995) The product of the ataxia-telangiectasia group D complementing gene, *ATDC*, interacts with a protein kinase C substrate and inhibitor. *Proc. Natl Acad. Sci. USA*, **92**, 7824–7828.
26. Wu, L.C., Wang, Z.W., Tsan, J.T., Spillman, M.A., Phung, A., Xu, X.L., Yang, M.-C.W., Hwang, L.-Y., Bowcock, A.M. and Baer, R. (1996) Identification of a RING protein that can interact *in vivo* with the *BRCA1* gene product. *Nature Genet.*, **14**, 430–440.
27. Lupas, A. (1996) Coiled coils: new structures and new functions. *Trends Biochem. Sci.*, **21**, 375–382.
28. Ishii, T., Aoki, N., Noda, A., Adachi, T., Nakamura, R. and Matsuda, T. (1995) Carboxy-terminal cytoplasmic domain of mouse butyrophilin specifically associates with a 150-kDa protein of mammary epithelial cells and milk fat globule membrane. *Biochim. Biophys. Acta*, **1245**, 285–292.
29. Perez, A., Kastner, P., Sethi, S., Lutz, Y., Reibel, C. and Chambon, P. (1993) PMLRAR homodimers: distinct DNA binding properties and heteromeric interactions with RXR. *EMBO J.*, **12**, 3171–3182.
30. Shou, W., Li, X., Wu, C.F., Cao, T., Kuang, J., Che, S. and Etkin, L.D. (1996) Finely tuned regulation of cytoplasmic retention of *Xenopus* nuclear factor 7 by phosphorylation of individual threonine residues. *Mol. Cell. Biol.*, **16**, 990–997.
31. Grignani, F., Testa, U., Rogaia, D., Ferrucci, P.F., Samoggia, P., Pinto, A., Aldinucci, D., Gelmetti, V., Fagioli, M., Alcalay, M., Seeler, J., Nicoletti, I., Peschle, C. and Pelicci, P.G. (1996) Effects on differentiation by the promyelocytic leukemia PML/RARalpha protein depend on the fusion of the PML protein dimerization and RARalpha DNA binding domains. *EMBO J.*, **15**, 4949–4958.
32. Grignani, F., Fagioli, M., Alcalay, M., Longo, L., Pandolfi, P.P., Donti, E., Biondi, A., Lo Coco, F., Grignani, F. and Pelicci, P.G. (1994) Acute promyelocytic leukemia: from genetics to treatment. *Blood*, **83**, 10–25.
33. Le Douarin, B., Zechel, C., Garnier, J.M., Lutz, Y., Tora, L., Pierrat, P., Heery, D., Gronemeyer, H., Chambon, P. and Losson, R. (1995) The N-terminal part of TIF1, a putative mediator of the ligand-dependent activa-

tion function (AF-2) of nuclear receptors, is fused to B-raf in the oncogenic protein T18. *EMBO J.*, **14**, 2020–2033.
34. Reddy, B.A., Kloc, M. and Etkin, L. (1991) The cloning and characterization of a maternally expressed novel zinc finger nuclear phosphoprotein (xnf7) in *Xenopus laevis*. *Dev. Biol.*, **148**, 107–116.
35. Sackett, D.L. (1995) Vinca site agents induce structural changes in tubulin different from and antagonistic to changes induced by colchicine site agents. *Biochemistry*, **34**, 7010–7019.
36. Mu, Z.M., Chin, K.V., Liu, J.H., Lozano, G. and Chang, K.S. (1994) PML, a growth suppressor disrupted in acute promyelocytic leukemia. *Mol. Cell. Biol.*, **14**, 6858–6867.
37. Fagioli, M., Alcalay, M., Tomassoni, L., Ferrucci, P.F., Mencarelli, A., Riganelli, D., Grignani, F., Pozzan, T., Nicoletti, I. and Pelicci, P.G. (1998) Cooperation between the RING + B1–B2 and coiled-coil domains of PML is necessary for its effects on cell survival. *Oncogene*, **16**, 2905–2913.
38. Borden, K.L.B., Lally, J.M., Martin, S.R., O'Reilly, N.J., Solomon, E. and Freemont, P.S. (1996) *In vivo* and *in vitro* characterization of the B1 and B2 zinc-binding domains from the acute promyelocytic leukemia protooncoprotein PML. *Proc. Natl Acad. Sci. USA*, **93**, 1601–1606.
39. Cao, T., Borden, K.L., Freemont, P.S. and Etkin, L.D. (1997) Involvement of the rfp tripartite motif in protein–protein interactions and subcellular distribution. *J. Cell Sci.*, **110**, 1563–1571.
40. Vortkamp, A., Gessler, M. and Grzeschik, K.-H. (1991) *GLI3* zinc finger gene interrupted by translocations in Grieg syndrome families. *Nature*, **352**, 539–540.
41. Wild, A., Kalff-Suske, M., Vortkamp, A., Bornholdt, D., Konig, R. and Grzeschik, K.H. (1997) Point mutations in human GLI3 cause Greig syndrome. *Hum. Mol. Genet.*, **6**, 1979–1984.
42. Kang, S., Graham, J.M.Jr, Olney, A.H. and Biesecker, L.G. (1997) GLI3 frameshift mutations cause autosomal dominant Pallister–Hall syndrome. *Nature Genet.*, **15**, 266–268.
43. Radhakrishna, U., Wild, A., Grzeschik, K.H. and Antonarakis, S.E. (1997) Mutation in GLI3 in postaxial polydactyly type A [letter]. *Nature Genet.*, **17**, 269–271.
44. Biesecker, L.G. (1997) Strike three for GLI3 [published erratum appears in *Nature Genet.* (1998) **18**, 88]. *Nature Genet.*, **17**, 259–260.
45. Shin, S.H., Kogerman, P., Lindstrøm, E., Toftgørd, R. and Biesecker, L.G. (1999) GLI3 mutations in human disorders mimic *Drosophila* Cubitus interruptus protein functions and localization. *Proc. Natl Acad. Sci. USA*, **96**, 2880–2884.
46. Sisson, J.C., Ho, K.S., Suyama, K. and Scott, M.P. (1997) Costal2, a novel kinesin-related protein in the Hedgehog signaling pathway. *Cell*, **90**, 235–245.
47. Robbins, D.J., Nybakken, K.E., Kobayashi, R., Sisson, J.C., Bishop, J.M. and Therond, P.P. (1997) Hedgehog elicits signal transduction by means of a large complex containing the kinesin-related protein costal2. *Cell*, **90**, 225–234.
48. Rugarli, E.I., Ghezzi, C., Valsecchi, V. and Ballabio, A. (1996) The Kallmann syndrome gene product expressed in COS cells is cleaved on the cell surface to yield a diffusible component. *Hum. Mol. Genet.*, **5**, 1109–1115.
49. Evan, G.I., Lewis, G.K., Ramsay, G. and Bishop, J.M. (1985) Isolation of monoclonal antibodies specific for human c-*myc* proto-oncogene product. *Mol. Cell. Biol.*, **5**, 3610–3616.
50. Graham, F.L. and Van der Eb, A.J. (1973) A new technique for the assay of infectivity of human adenovirus 5 DNA. *Virology*, **2**, 456–464.